Available online at www.sciencedirect.com
SCIENCE DIRECT
Journal of Molecular Structure 780–781 (2006) 7–16
Journal of MOLECULAR STRUCTURE
www.elsevier.com/locate/molstruc

Tunable diode laser measurements of N_2- and O_2-pressure broadening and pressure-induced shifts for $^{16}O^{12}C^{32}S$ transitions in the ν_3 band

M.A. Koshelev[a], M.Yu. Tretyakov[a], R.M. Lees[b,*], L.-H. Xu[b]

[a]*Institute of Applied Physics of Russian Academy of Sciences, 46 Uljanova Str., Nizhnii Novgorod 603950, Russian Federation*
[b]*Department of Physical Sciences, Canadian Institute for Photonic Innovations (CIPI) and Centre for Laser, Atomic and Molecular Sciences (CLAMS), University of New Brunswick, Saint John, N.B., Canada E2L 4L5*

Received 10 December 2004; revised 16 March 2005; accepted 21 March 2005
Available online 6 September 2005

Abstract

Nitrogen and oxygen pressure broadening and pressure-induced shift coefficients for 42 transitions of $^{16}O^{12}C^{32}S$ with quantum number m from -25 to 49 in the P and R branches of the ν_3 band at 2062 cm^{-1} have been measured at room temperature using a high-resolution tunable diode laser spectrometer. Air-broadening and shift parameters have also been calculated from the N_2 and O_2 measurements. The dependence of the broadening and shifting on rotational quantum number is discussed. The results are compared to previous measurements in the ν_1 and $2\nu_3$ bands and to the parameters for the ν_3 band that are reported in the HITRAN database.

Keywords: OCS molecule; IR spectroscopy; Mid-IR TDL spectrometer; Pressure broadening; Pressure-induced shifts; Air broadening; Line intensities

1. Introduction

This paper reports pressure broadening and pressure-induced shift measurements for transitions of the ν_3 band of the linear OCS molecule in mixtures with N_2 and O_2. OCS is an important environmental molecule, as it is one of the principal and most long-lived reservoirs of sulfur in the Earth's atmosphere [1–5] and has also been detected in the atmosphere of Venus [6,7], the Orion molecular cloud [8], and in comets Hyakutake and Hale-Bopp [9,10]. Such observations have mainly involved spectral transitions belonging to the strong ν_3 absorption band centered at 2062.2 cm^{-1}, which corresponds to the O=C stretching vibrational mode of the molecule. In particular, the ν_3 band of OCS has been used for concentration measurements of carbonyl sulfide in the upper troposphere and lower stratosphere of the Earth and for long-term trend measurements of column abundances and mixing ratios [4,5]. The ν_3 band is also a candidate for use with space and ground-based techniques for investigation of the Martian atmosphere [11]. However, the accuracy of information retrieval from such remote sensing measurements depends critically on a precise knowledge of the spectroscopic parameters for the transitions of the band. Thus, accurate OCS line positions, intensities, and pressure broadening and pressure shift coefficients are essential data for reliable probing of the Earth's atmosphere and the variety of astronomical OCS sources.

Due to their special importance for frequency calibration purposes in the 5 μm region, line position measurements for the ν_3 band of OCS have been pursued for some time (e.g. in [12]), and extensive tables have been compiled by Maki and Wells [13]. Line intensities in the ν_3 band were also reported recently by Régalia-Jarlot et al. [14] from a Fourier transform infrared (FTIR) study. However, relatively few measurements of the nitrogen and oxygen pressure broadening and shift parameters have been published, and those are for the ν_1 and $2\nu_3$ bands [15–17]. The OCS air-broadening coefficients tabulated in the GEISA [18] and HITRAN databases [19] are based on the ν_1 band measurements performed in 1985 [15] and 1987 [16], and no data on pressure shifts are included.

The need for more extensive experimental information for the ν_3 band motivated our present study of OCS line broadening by nitrogen and oxygen, employing

* Corresponding author. Tel.: +1 506 648 5864; fax: +1 506 648 5948.
E-mail address: lees@unb.ca (R.M. Lees).

0022-2860/$ - see front matter © 2005 Elsevier B.V. All rights reserved.
doi:10.1016/j.molstruc.2005.03.056

the mid-infrared tunable diode laser (IR TDL) spectrometer at the University of New Brunswick in Saint John. In this paper, we report room temperature measurements of the N_2 and O_2 pressure broadening and pressure shift coefficients for 42 transitions of the ν_3 band. The quantum number range investigated covers m values from -25 for the P-branch up to 49 for the R-branch ($m=-J$ for the P-branch and $m=J+1$ for the R-branch, where J is the rotational quantum number of the lower level). Nitrogen and oxygen were chosen as perturbing gases as being the two main constituents of the Earth's atmosphere. The broadening and shift parameters for dry air are also calculated from the measured N_2 and O_2 parameters assuming binary collisions and a 79/21 percent atmospheric ratio of N_2 to O_2 [20]. A comparison of our data with previous measurements and the HITRAN compilation is presented, and possible causes of uncertainties and discrepancies are discussed.

2. Experimental aspects

The IR TDL spectrometer employed for the present measurements is based on the commercial Laser Photonics L5000 package [http://www.lasercomponents.com/] described in [21]. A block diagram of the experimental layout, highlighting the features used for frequency calibration and signal detection, is shown in Fig. 1. The source of coherent radiation was a lead–salt laser diode (Model L5621-2024) cooled by liquid nitrogen (LN_2). Variation of the diode temperature (85–115 K) and current via the L5830 Digital Controller permitted operation over the region from 2024 to 2079 cm^{-1} with small gaps due to mode hops. The laser beam was split into three parts, with the main beam being directed into the sample cell and the other two beams used for frequency calibration as described below.

Customarily in TDL systems, a Fabry–Perot etalon in combination with a reference spectrum is used for frequency calibration. However, as was discussed in [21], the achievable calibration accuracy using an etalon with free spectral range of 0.02997 cm^{-1} is of the order of 0.001–0.002 cm^{-1} for LN_2-cooled diodes, insufficient for accurate investigation of absorption lineshapes where the effects of foreign gas broadening and pressure shifting are small. However, it was shown in [21] that improved calibration accuracy (better than 0.0002 cm^{-1}) over the full width of the laser scan could be achieved by using a reference spectrum with a suitable distribution of peaks. The OCS molecule has a very rich spectrum (about 45 and 35 lines/cm^{-1} in the center and at the edges of the ν_3 region, respectively [13]) due to the presence of numerous isotopic and combination bands, and so is very suitable for calibration purposes. Furthermore, the line center positions have been measured with high precision to better than $5–10^{-5}$ cm^{-1} for strong transitions and 10^{-4} cm^{-1} for weak transitions and are readily available in extensive on-line calibration tables [13].

In our present work, therefore, we followed the frequency calibration scheme recommended in [21] but with dual reference cells. The first was a 1 m multipass White cell for long-path observations of 'weak' transitions (intensity $<10^{-19}$ cm^{-2}/molecule) and the second a short

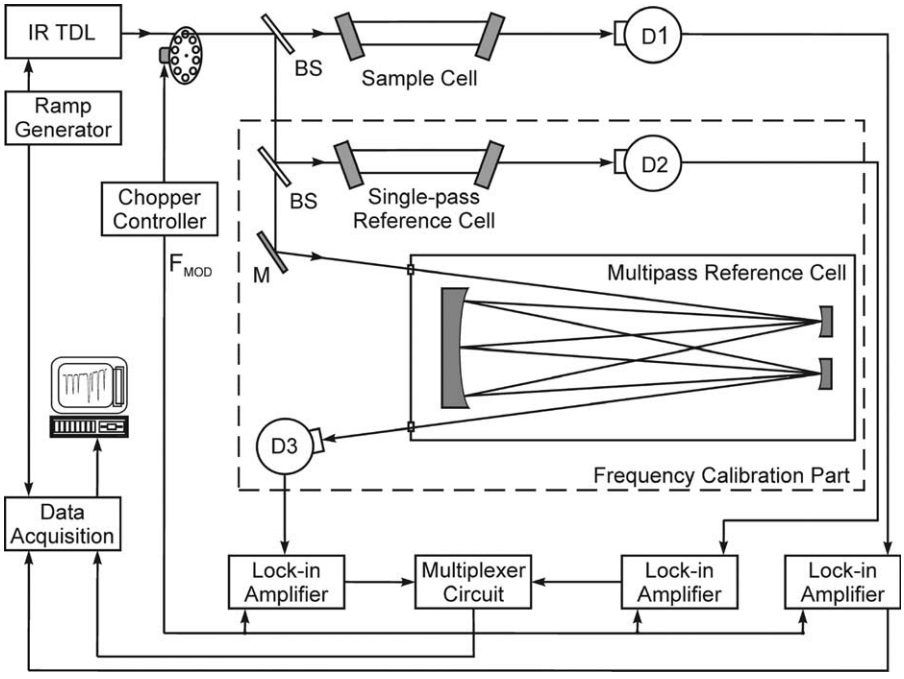

Fig. 1. Block layout of the experimental IR TDL spectrometer, showing the data acquisition and frequency calibration schemes. BS, beamsplitter; M, mirror; D, detector; F_{MOD}, amplitude-modulation chopping frequency used as the reference frequency for the lock-in amplifiers operating in 1-f mode.

single-pass cell for 'strong' lines (intensity $>10^{-19}$ cm^{-2}/molecule), as shown in Fig. 1. In our measurements, we set the multipass cell to 8 transits to give an 8 m path length and used an OCS pressure of 30–50 mTorr, as measured on a Baratron capacitance gauge. At this combination of long path length and modest OCS pressure, the 'weak' lines were seen with high signal-to-noise (*S*/*N*) ratio with linewidths corresponding just to the Doppler HWHM of about 0.00163 cm^{-1}, but the 'strong' lines were heavily saturated and had much larger widths. To obtain accurate calibration frequencies for the 'strong' lines, therefore, the 16 cm single-pass reference cell was used with an OCS pressure of about 100 mTorr.

To provide enough (7–10) OCS reference lines for precise frequency calibration, we recorded the spectrum over a range of about 0.2–0.3 cm^{-1} in the vicinity of each target $^{16}O^{12}C^{32}S$ transition under study. Multiple scans were digitally averaged to give the final spectral record, and each record was repeated twice to check the reproducibility and to give an estimate of the statistical errors in the measurements.

For the measurement of the pressure broadening and pressure shifts, we employed a 16 cm single-pass sample cell with OCS partial pressures in the range from 70 to 110 mTorr, depending on the intensity of the target $^{16}O^{12}C^{32}S$ transition. For each target transition, the line profile was recorded for 9–12 different pressures of the perturbing N_2 and O_2 foreign gases over the range from 30 to 110 Torr. Where neighboring transitions of significant strength lay close to the target line, the upper pressure limit was reduced down to 70 Torr to avoid complications from line overlapping. Throughout the measurements, the absorption cell was connected to a 1 l ballast volume and to the vacuum system, and the total pressure was measured with a Type 750B MKS Baratron gauge having a 1000 Torr full scale reading and a stated accuracy of 1%. The initial OCS pressure in the system and sample cell for each target line was measured with a Model 375 Convectron vacuum gauge calibrated for OCS against a Baratron gauge. The N_2 and O_2 gases (purity > 99.99 vol%) were provided by Air Liquide, Inc., and the OCS samples were drawn directly from a Matheson lecture bottle with purity believed to be better than 99.9%.

After each change of pressure, we delayed starting a new record for a period of about 15 min, corresponding to approximately five characteristic relaxation times for the gas to reach a uniform distribution in the vacuum system and sample cell. The relaxation time was estimated from test measurements of variation in line half-width versus elapsed time in which several rapidly repeated recordings of the absorption line were made immediately after a pressure change.

The experiment was carried out at room temperature as measured with a digital Micronta thermometer with 0.1 °C display resolution and 1 °C accuracy and also a standard mercury thermometer with 1 °C scale factor. Both readings coincided well, and varied within the range from 22 to 25.5 °C from day to day. Temperature variations during the measurements on any given day did not exceed 1 °C.

The laser beams passing through the multipass and sample cells were detected by LN_2-cooled HgCdTe detectors; an InSb detector was used for the single-pass reference signal. The beams were chopped at 3 kHz and the output signals from the detectors were demodulated by lock-in amplifiers in 1-*f* mode to give the transmittances for the three channels. The laser frequency was swept by applying a 0.5 Hz ramp voltage to the external modulation input of the L5830 controller, with amplitude selected to give a laser frequency scan speed of about 0.1–0.15 cm^{-1}/s. A lock-in amplifier time constant of 3 ms was found to give optimum balance between low instrumental distortion of the line-shape and high *S*/*N* ratio.

The spectra were captured into the computer using a CompuScope-1012 two-channel A/D data acquisition card at a sampling frequency of 500 Hz. One channel was used solely for the sample spectrum, while the other was switched via a multiplexer circuit between the two reference spectra in successive sweeps. Thus, the first channel contained repeated sample spectra while the second had alternating calibration spectra. Our in-house data processing program permits multi-scan averaging, hence each spectrum was averaged over 25 scans and consisted of 1000 points. Fig. 2 shows an example of a raw experimental record in the vicinity of the *R*(40) line of OCS at 2073.7287 cm^{-1}. The upper trace from the first channel corresponds to the repeated sample spectrum recorded at an O_2 pressure of 90.93 Torr and an OCS partial pressure of about 110 mTorr. The middle trace from the second channel consists of the calibration spectra from the multipass (first half) and single-pass (second half) reference cells. The bottom trace shows the ramp signal from the signal generator.

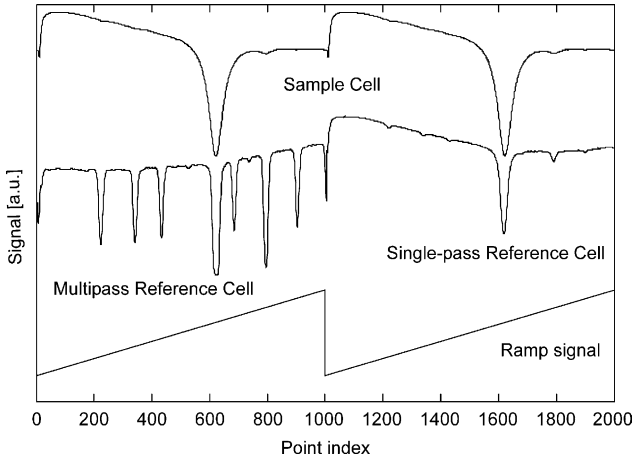

Fig. 2. Raw experimental record of the OCS spectrum in the vicinity of the *R*(40) line at 2073.7287 cm^{-1}. Upper trace shows repeated records of the sample cell spectrum for a mixture of approximately 100 mTorr of OCS broadened by 90.93 Torr of O_2. Middle trace shows the alternating multiplexed records for the multipass (first sweep) and single-pass (second sweep) reference cells. Ramp signal is shown at the bottom of the figure.

For each target line studied, the following records were made consecutively under the same laser sweep conditions: (1) an empty-cell background spectrum (giving the 100% transmission level) representing the laser emission profile, interference effects, etc.; (2) a spectrum at low pressure (< 40 mTorr) of pure OCS, giving the OCS Doppler profile convolved with the TDL instrumental function; (3) a spectrum of the saturated line at high OCS pressure, giving the 0% transmission level; (4) spectra of the broadened line at several pressures of the perturbing foreign gas; (5) a repeated empty-cell background spectrum.

The background spectra had *S*/*N* ratios ranging from 3000 to 5000, and were recorded at both the beginning and the end of a measurement sequence to allow correction for baseline changes due to temperature drifts. Such changes were usually no more than 2–3% and were observed to be essentially proportional to elapsed time, hence corrections could be made by interpolating between initial and final background spectra assuming a linear change with time. Also, since test background traces with different pressures of pure nitrogen and oxygen in the sample cell did not reveal any changes in the signal, the background recordings were made only with the cell evacuated.

Examples of typical experimental records in a sequence are shown overlaid in Fig. 3, again for the *R*(40) line of OCS. The background trace and the recording of the low-pressure pure OCS spectrum are displayed at the top, and then four sample O_2-broadened spectra at O_2 pressures of 37.97, 60.60, 75.62 and 97.60 Torr. For clarity, the saturated spectrum of the high-pressure pure OCS is not shown explicitly in Fig. 3, but the 0% transmission level derived from the signal at the center of the saturated line is indicated at the bottom.

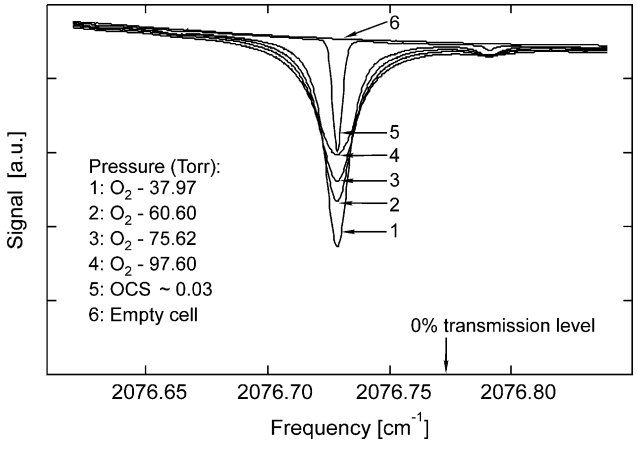

Fig. 3. Examples of experimental O_2-broadened spectra obtained for the *R*(40) line of OCS. Traces 1–4 are for mixtures of approximately 100 mTorr of OCS with increasing O_2 pressures of 37.97, 60.60, 75.62 and 97.60 Torr, respectively; Trace 5 is a record of the line at a lower pressure of 30 mTorr of pure OCS; Trace 6 is a background record (100% transmission level). The 0% transmission level was determined from a record of the saturated line at high pressure of pure OCS.

3. Data treatment and experimental results

Data treatment started with the laser frequency calibration procedure. First of all, the first 100–150 points were deleted from each record to remove the initial transients seen in Fig. 2 that arise following the flyback in the sweep. The two repeated sample spectra were also averaged at this time. The results of this processing for the raw traces of Fig. 2 are shown in Fig. 4 for the *R*(40) OCS line. The point indices of the center positions of all the calibration transitions were then plotted against their standard reference frequencies from [13] and fitted to a fourth-order polynomial. The fitted calibration curve for the *R*(40) line and the fit residuals are shown in the middle and lower parts of Fig. 4, respectively. The standard deviation of the fit was 0.7×10^{-5} cm^{-1}, which is comparable to the reference data accuracies reported in [13].

Next, the calibrated OCS transition profiles were analyzed to obtain the line widths and center frequencies as functions of the pressure of the foreign gas perturber. The absorption coefficient $\alpha(\nu)$ at frequency ν is defined through

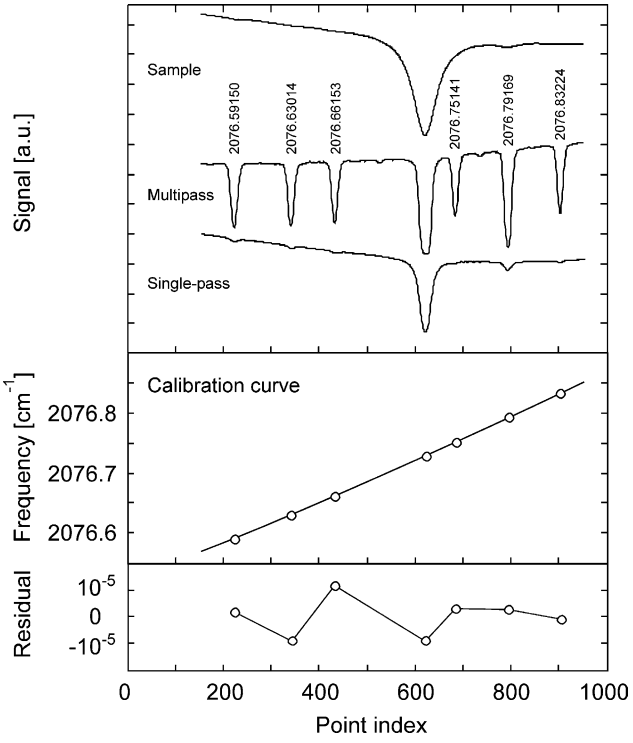

Fig. 4. Calibration of the spectra in the vicinity of the *R*(40) line of OCS. Upper traces show the results obtained from the experimental spectra of Fig. 2 after averaging of the repeated sample signals and deletion of the first 150 and last 50 points from each record. Line frequencies shown above the multipass reference cell spectrum are taken from [13]. Calibration points mapping the point index of the reference peaks against their absolute frequencies from [13] are shown in the middle figure by open circles. The solid line represents a fourth-degree polynomial fit to the data. The residuals of the fit on a magnified scale are shown at the bottom.

the Beer–Lambert Law as

$$I(v) = I_0(v)e^{-a(v)\times L} \quad (1)$$

where $I(\nu)$ and $I_0(\nu)$ are the transmitted and incident radiation power, respectively, and L is the optical path length. For each spectral record, we took the $I_0(\nu)$ values as the difference between background (100%) and saturated (0%) signals, determined $I(v)$ at each point, and then calculated the experimental absorption coefficient profile as proportional to $-\ln[I(\nu)/I_0(\nu)]$. To obtain the parameters of the transitions, the following model function based on the Voigt profile was fitted to the experimental profile

$$\alpha(v) = \left[A_0 \int_{-\infty}^{\infty} \frac{\exp(-\tau)}{y^2 + (x-\tau)^2} d\tau [1 + A_1(v - v_0)]\right] + A_2 + A_3(v - v_0) \quad (2)$$

where

$$y = \frac{\gamma_C}{\gamma_{Deff}}\sqrt{\ln(2)} \quad \text{and} \quad x = \frac{v - v_0}{\gamma_{Deff}}\sqrt{\ln(2)}.$$

Here, γ_C is the collisional line half-width at half maximum (HWHM), γ_{Deff} is an 'effective' Doppler HWHM, and ν_0 is the line center frequency. A_0, A_1, A_2 and A_3 are adjustable coefficients as are x, y and ν_0. The linear A_1 multiplicative term and the constant A_2 and linear A_3 additive terms are included to take account of the background plus the wings of any neighboring lines.

The effective Doppler width was determined from the second spectrum of each sequence recorded at low OCS pressure (about 20–30 mTorr) to check the effect of a finite instrumental bandwidth for the TDL arising from diode temperature and current fluctuations. The low-pressure line profile was modeled as a convolution of a Gaussian Doppler profile of half-width γ_D and an instrumental function also assumed to be Gaussian [22] with a half-width γ_{inst}. (At that pressure, the ratio of Doppler to collisional half-widths is about 200 so that collisional broadening is negligible.) Since the convolution of two Gaussian functions is also a Gaussian, the 'effective' Doppler half-width γ_{Deff}, defined as $\gamma_{Deff} = \sqrt{\gamma_D^2 + \gamma_{inst}^2}$, was determined by fitting a Gaussian lineshape to the experimental record. The values obtained for γ_{Deff} were 5–12% higher than the calculated γ_D of 0.00163 cm^{-1}, corresponding to γ_{inst} values from 0.0005(1) to 0.0008(1) cm^{-1} depending on the operating temperature and current.

In fitting each pressure-broadened molecular line profile to Eq. (2), a section of spectral record covering about six line half-widths was used in order to obtain accurate line shape parameters, and from 100 to 300 points were fitted per spectral record depending on the pressure of the perturbing gas. Fig. 5 shows a typical fit of the model function (2) to an experimental record, in this case for the $R(40)$ OCS line broadened by 66 Torr of N_2. The residuals of the fit are shown at the bottom of the figure. The signal-to-noise ratio,

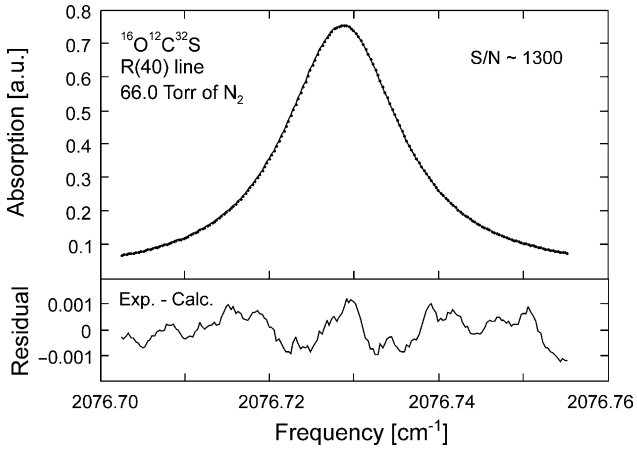

Fig. 5. Fitting of the calibrated absorption spectrum of the $R(40)$ line of OCS broadened by 66 Torr of nitrogen. The solid line shows the fit of the model function of Eq. (2) to the experimental points. The observed-minus-calculated residuals of the fit are displayed underneath on a magnified scale. Line parameters determined from the fit are 2076.72854(1) cm^{-1} for the line center position and 0.00772(1) cm^{-1} for the collisional HWHM. The estimated signal-to-noise ratio is about 1300.

determined as the ratio of the line amplitude to the standard deviation of the residuals, is equal to 1300 for the record shown. The line center position and HWHM were obtained as 2076.72854(3) and 0.00772(3) cm^{-1}, respectively, where the uncertainties shown in parentheses correspond to 3-σ deviations in the last digit.

The fit residuals in Fig. 5 show some traces of the characteristic discrepancies found for the Voigt model when the effects of velocity-changing collisions start to become

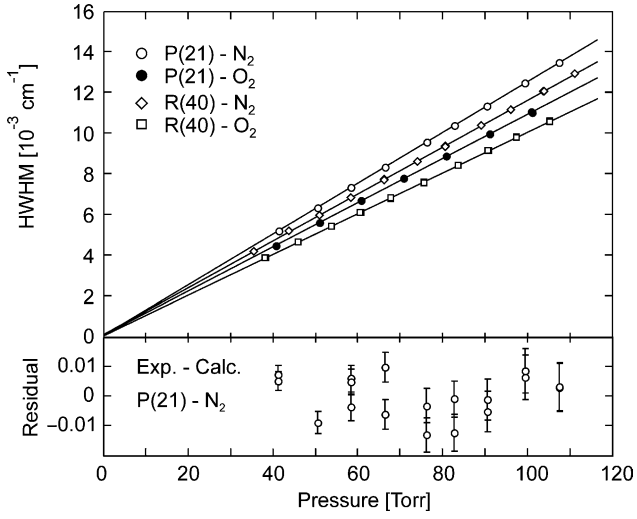

Fig. 6. N_2- and O_2-pressure dependence of the collisional HWHM (in units of 10^{-3} cm^{-1}) for the $P(21)$ and $R(40)$ lines of OCS. The solid lines represent linear regressions to the experimental points. The slopes of the lines were determined as 0.0953(10) and 0.0871(10) cm^{-1} atm^{-1} for N_2 broadening and as 0.0830(10) and 0.0745(10) cm^{-1} atm^{-1} for O_2 broadening of the $P(21)$ and $R(40)$ lines, respectively. The residual of the fit for the N_2-dependence of the $P(21)$ linewidth is shown underneath, with error bars corresponding to 1-σ uncertainties in the experimental halfwidths.

important (see [23], for example). Therefore, several test calculations were carried out employing the more general Galatry profile [24] and were found to improve the residuals by a factor of about 2–3 due to the additional adjustable parameter at the cost of greatly increased computational time. However, there were no significant changes in the fitted linewidths to within our experimental uncertainties.

The fitted collisional half-widths γ_C are plotted as a function of the pressure of the gas mixture in Fig. 6 for the examples of the $P(21)$ and $R(40)$ transitions. The data were fitted by linear regression to give the pressure broadening coefficients as the slopes of the lines. The residuals for the fit to the N_2-broadening data for the $P(21)$ line are shown at the bottom of Fig. 6 with error bars corresponding to 1-σ uncertainties in the experimental half-widths. The low level of scatter about zero demonstrates the excellent linearity of the plots as well as the good reproducibility of the measurements. Values of approximately 0.1×10^{-3} cm^{-1} were obtained for the intercepts at zero pressure in Fig. 6, about half of which can be accounted for from self-

Table 1
Measured pressure broadening and shift parameters for transitions in the ν_3 band of OCS[a]

Transition	Pressure broadening γ			Pressure shift δ		
	N_2	O_2	Air[b]	N_2	O_2	Air[c]
P(25)	93.5(15)	80.4(15)	90.7(15)	−3.3(3)	−2.2(3)	−3.1(3)
P(24)	93.9(14)	81.2(10)	91.2(13)	−4.8(16)	−3.1(5)	−4.4(14)
P(23)	94.9(10)	81.9(10)	92.2(10)	−3.3(6)	−2.6(3)	−3.2(5)
P(21)	95.3(10)	83.0(10)	92.7(10)	−1.8(3)	−2.1(2)	−1.9(3)
P(20)	96.6(10)	83.3(11)	93.8(10)	−5.5(28)	−1.1(10)	−4.6(24)
P(18)	97.6(10)	84.1(10)	94.8(10)	−3.2(3)	−1.4(5)	−2.8(3)
P(17)	97.9(10)	85.4(10)	95.3(10)	−2.3(3)	−3.6(3)	−2.6(3)
P(15)	97.9(10)	85.4(10)	95.3(10)	−5.3(8)	−3.0(6)	−4.8(8)
P(14)	99.0(15)	86.3(10)	96.3(14)	−5.2(8)	−1.4(5)	−4.4(7)
P(13)	98.9(10)	87.0(12)	96.4(10)	−1.4(22)	−2.0(5)	−1.5(18)
P(12)	99.4(11)	86.8(10)	96.8(11)	−2.2(7)	−1.5(5)	−2.1(7)
P(11)	99.9(10)	87.6(10)	97.3(10)	−1.7(18)	−2.4(5)	−1.8(15)
P(8)	102.0(6)	89.5(12)	99.4(7)	−2.0(4)	−2.1(6)	−2.0(4)
P(7)	102.5(11)	90.4(12)	100.0(11)	−2.9(5)	−2.2(4)	−2.8(5)
P(6)	103.4(10)	90.6(10)	100.7(10)	−4.2(4)	−4.4(4)	−4.2(4)
P(5)	104.6(10)	91.5(10)	101.9(10)	−1.8(14)	−0.7(4)	−1.6(12)
P(4)	104.9(8)	92.1(10)	102.2(8)	−2.8(11)	−3.8(5)	−3.0(10)
P(3)	106.1(14)	93.4(10)	103.4(13)	−0.8(7)	−1.2(5)	−0.9(7)
R(1)	107.8(10)	94.8(10)	105.1(10)	−1.8(5)	−1.2(7)	−1.7(5)
R(2)	105.9(15)	93.3(15)	103.2(15)	−0.8(10)	−1.7(21)	−1.0(12)
R(3)	104.9(13)	92.5(15)	102.3(13)	−4.5(4)	−1.7(8)	−3.9(5)
R(4)	103.9(12)	90.9(10)	101.2(12)	−4.6(6)	−3.0(7)	−4.3(6)
R(7)	102.1(10)	89.1(10)	99.4(10)	−2.7(4)	−2.4(8)	−2.6(5)
R(8)	101.3(10)	89.1(12)	98.8(10)	−2.8(4)	−2.1(2)	−2.7(4)
R(9)	100.4(12)	88.1(12)	97.9(12)	−0.8(5)	−1.3(2)	−0.9(4)
R(14)	98.4(10)	85.8(10)	95.7(10)	−2.3(7)	−1.7(3)	−2.2(6)
R(15)	98.2(12)	85.6(10)	95.5(12)	−2.1(3)	−2.3(3)	−2.1(3)
R(16)	97.7(10)	85.0(10)	95.0(10)	−2.3(6)	−1.6(4)	−2.2(6)
R(17)	97.0(10)	84.4(10)	94.3(10)	−1.5(5)	−1.9(7)	−1.6(5)
R(27)	91.6(10)	78.9(10)	89.0(10)	−1.5(5)	−2.2(4)	−1.6(5)
R(28)	91.2(12)	78.5(12)	88.6(12)	−2.4(4)	−2.5(4)	−2.4(4)
R(29)	91.2(10)	78.0(15)	88.5(11)	−4.2(5)	−1.5(7)	−3.6(5)
R(33)	89.3(13)	76.7(10)	86.7(12)	−1.6(6)	−1.2(10)	−1.5(7)
R(34)	89.3(10)	76.6(10)	86.6(10)	−2.4(4)	−2.8(4)	−2.5(4)
R(35)	88.5(13)	76.1(10)	85.9(12)	−3.8(5)	−1.7(3)	−3.4(5)
R(37)	88.1(10)	75.8(10)	85.5(10)	−1.5(4)	−2.8(6)	−1.8(4)
R(38)	87.8(10)	75.2(14)	85.1(11)	−2.5(5)	−1.8(5)	−2.4(5)
R(39)	87.2(10)	74.7(10)	84.6(10)	−3.6(3)	−2.9(8)	−3.5(4)
R(40)	87.1(10)	74.5(10)	84.4(10)	−3.4(6)	−2.9(4)	−3.3(6)
R(46)	85.7(10)	72.7(10)	83.0(10)	−2.8(4)	−2.4(3)	−2.7(4)
R(47)	85.5(10)	72.2(10)	82.7(10)	−2.6(5)	−2.5(5)	−2.6(5)
R(48)	85.4(10)	72.3(10)	82.7(10)	−2.9(6)	−1.8(3)	−2.7(5)

[a] Pressure broadening and shift coefficients are both in units of 10^{-3} cm^{-1} atm^{-1}. Uncertainties in parentheses correspond to three standard deviations (3-σ) in the last digit.

[b] Calculated from the measured N_2 and O_2 parameters as $\gamma^{Air} = 0.79\gamma^{N_2} + 0.21\gamma^{O_2}$ [20].

[c] Calculated from the measured N_2 and O_2 parameters as $\delta^{Air} = 0.79\delta^{N_2} + 0.21\delta^{O_2}$.

broadening of the transitions. This closeness of the intercept values to zero serves to support the reliability of the data and the fitting procedures.

The values determined in the present work for the N_2- and O_2-broadening parameters γ^{N2} and γ^{O2} are presented in Table 1, together with those for the air-broadening parameter γ^{Air} calculated as [20]:

$$\gamma^{Air} = 0.79\gamma^{N_2} + 0.21\gamma^{O_2} \quad (3)$$

Since the data were obtained with slight variations in the room temperature over the range 22.0–25.5 °C, all the readings were normalized to a universal temperature of 23 °C using the exponent $n = 0.6$ from the HITRAN database [18] in the customary $(T_0/T)^n$ dependence for the broadening. The 3-σ uncertainties given in Table 1 appear to be realistic estimates of the actual experimental errors on the basis of observations of the reproducibility of the results for several test transitions over different days.

The strong variation of the N_2- and O_2-broadening parameters with rotational quantum number is shown in Fig. 7 as a function of the absolute value of m ($m = -J$ for the P-branch and $m = J+1$ for the R-branch). The data display a quite smooth dependence on quantum number, with good coincidence between transitions in the P- and R-branches having the same $|m|$. As expected, the broadening parameters decrease with increasing $|m|$, with minor irregularity in the vicinity of $m = 15$. Similar irregularity was seen for the N_2-, O_2- and air-broadening dependence on $|m|$ in the ν_1 vibrational band of OCS [15,16] as well as for other linear molecules, e.g. HCN [25].

Fig. 8 presents a comparison between our present results and those previously reported for OCS, with the regions lying within the 3-σ uncertainty limits of our measured ν_3 band data shown as grey zones. As may be seen in the upper and middle parts of Fig. 8, our measured N_2- and O_2-broadening coefficients are in reasonable agreement with

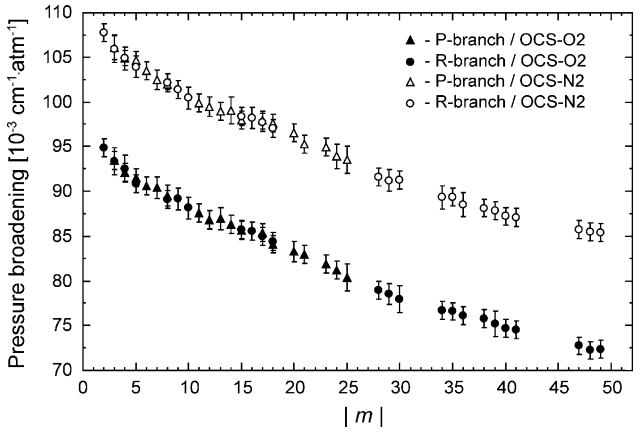

Fig. 7. Dependence of the measured N_2- and O_2-broadening coefficients on the rotational quantum number m for lines of the ν_3 band of OCS at 296 K. The N_2 data are shown as open triangles or circles for P-branch and R-branch lines, respectively, while the O_2 data are indicated by filled triangles and circles. The error bars correspond to 3-σ uncertainties in the experimental coefficients.

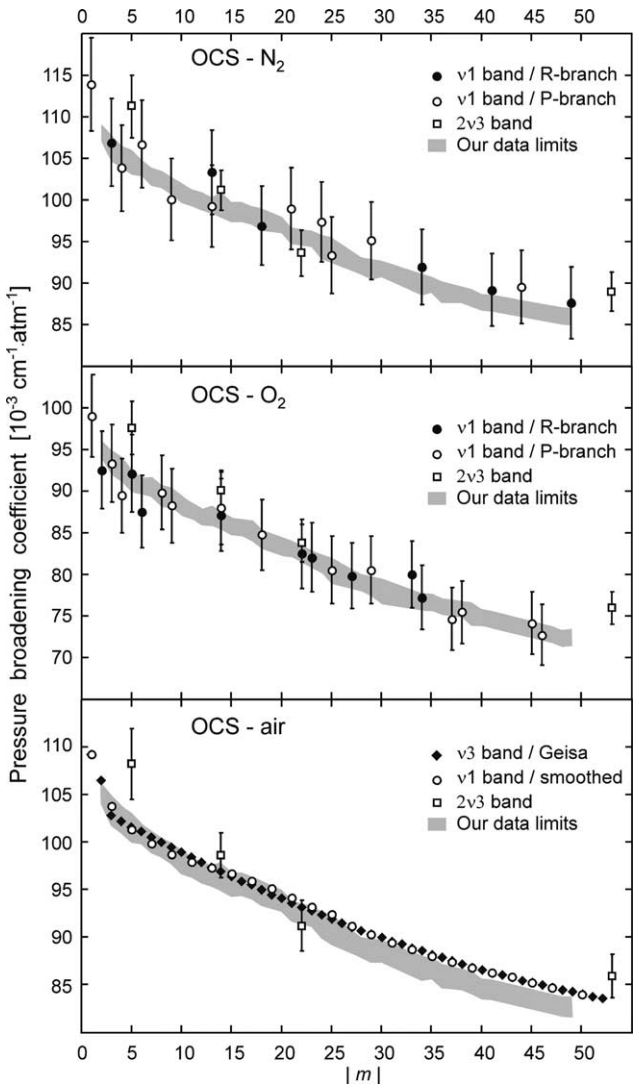

Fig. 8. N_2-, O_2- and air-broadening coefficients at 296 K plotted as a function of $|m|$. The grey zones show the 3-σ limits of our measured coefficients for both P- and R-branches of the ν_3 band of OCS. Data for the ν_1 band of OCS reported in [15,16] are shown by open (P-branch) and filled (R-branch) circles in the two upper pictures, with error bars corresponding to 5% uncertainty. Smoothed air-broadening parameters for lines of the ν_1 band are shown by open circles in the lower figure together with ν_3 band data from the GEISA database as filled diamonds. The open squares in all three graphs show the data reported in [17] for the $2\nu_3$ band of OCS.

those reported for both the ν_1 [15,16] and $2\nu_3$ [17] bands. The agreement with the ν_1 values is somewhat better for O_2 broadening than for N_2, possibly because of the treatment of the zero-pressure intercepts in the N_2 fitting in [16]. In Fig. 2 of [16] for the $P(21)$ line of the ν_1 band, it appears that the intercept at zero pressure was constrained to zero, although the first two points lie visibly above the fitted straight line of slope 98.6×10^{-3} cm^{-1} atm^{-1}. However, if we refit the linewidth data from [16] with an adjustable intercept, we find a value of 93.9×10^{-3} cm^{-1} atm^{-1} for the N_2-broadening coefficient, closer to our corresponding ν_3 value of 95.3×10^{-3} cm^{-1} atm^{-1}. The $2\nu_3$ line broadening

data [17] shown in Fig. 8 are also in general agreement with our results but have significantly larger uncertainties.

The bottom part of Fig. 8 compares our present ν_3 air-broadening coefficients to those for the ν_1 and $2\nu_3$ bands and also to those given for the ν_3 band in the GEISA database [18]. (Since the air-broadening parameters tabulated in the HITRAN database [19] are similar to those in the GEISA database [18], we show only the comparison for the latter.) The values for the ν_1 band at 296 K were taken directly from Table 2 of [15], while those for the $2\nu_3$ band were calculated from the N_2- and O_2-broadening data [16] using Eq. (3). Fig. 8 displays good agreement among the ν_1 and ν_3 data at lower m, but above $m=20$ our results are systematically lower, reaching a discrepancy of about 2.4% for m near 50. Although the ν_3 air-broadening coefficients tabulated in the GEISA database are similar to the ν_1 band data on which they are based [18], some small discrepancies are evident in Fig. 8. In particular, the apparent irregularity in the vicinity of $m=17$ seen here in Fig. 7 and mirrored in the ν_1 band data is absent from the GEISA curve. This would represent a potential source of error in use of the GEISA/HITRAN data.

In the upper part of Fig. 9, the ratio of O_2- to N_2-pressure broadening coefficients is plotted as a function of $|m|$. This ratio decreases monotonically with $|m|$ from 0.882 at low $|m|$ down to 0.844 at $|m|=50$. However, the difference between N_2- and O_2-pressure broadening parameters, shown at the bottom of Fig. 9, is independent of $|m|$ to within

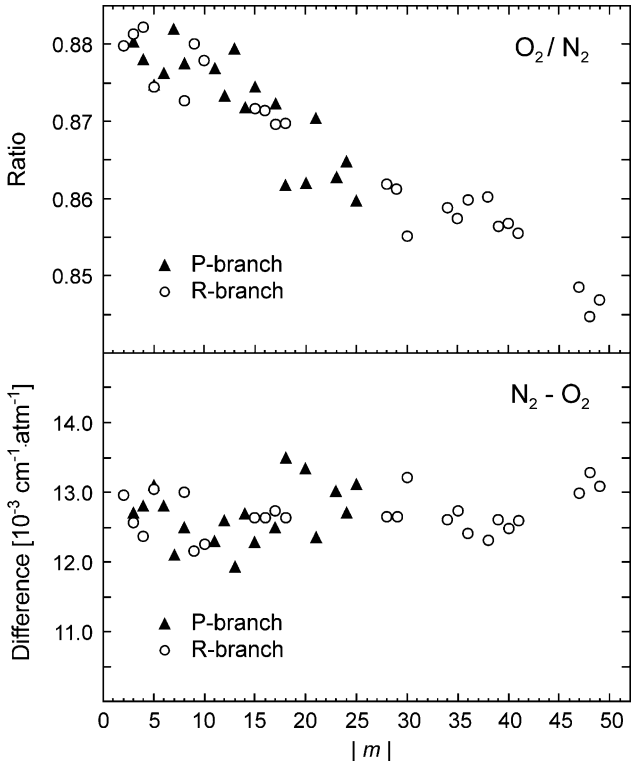

Fig. 9. Ratio of the O_2- to N_2-pressure broadening coefficients for lines of the ν_3 band of OCS at 296 K (upper figure) and difference between the coefficients (lower figure). P- and R-branch data are shown by filled triangles and open circles, respectively.

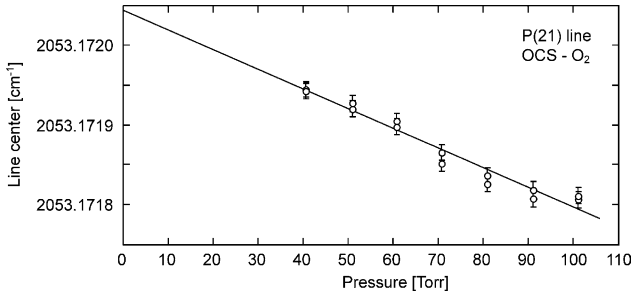

Fig. 10. Pressure dependence of the line center position for the O_2-broadened $P(21)$ line of OCS. Error bars indicate 1-σ uncertainties in the experimental values (open circles) obtained from fitting the observed spectra to the model function of Eq. (2). The solid line represents a linear regression to the data, with slope determined as $-0.0019(2)$ cm^{-1} atm^{-1}. The intercept at zero pressure is determined as 2053.172043(11) cm^{-1}, coinciding to within the uncertainty of our frequency calibration with the value of 2053.172006(1) cm^{-1} tabulated for the line center in [13].

experimental error and is equal to 0.0127(3) cm^{-1} atm^{-1} or about 15%. The ratio of air-broadening to N_2-broadening coefficients decreases from 0.975 at low $|m|$ to 0.967 for higher $|m|$, with a $(\gamma^{N_2}-\gamma^{air})$ difference of 0.00267(63) cm^{-1} atm^{-1}. This value coincides within our experimental error with that of 0.003 cm^{-1} atm^{-1} obtained for the ν_1 band [16], reinforcing the consistency between our results for the ν_3 band of OCS and those reported for the ν_1 band.

Turning to pressure shifts, we show in Fig. 10 the pressure dependence of the line center positions derived from fitting the model function (2) to the experimental records for the $P(21)$ line of OCS perturbed by O_2. A small negative shift linear with pressure is seen; the shift parameter δ determined from the slope of a linear regression to the experimental points is equal to $-0.0019(2)$ cm^{-1} atm^{-1} (with a 3-σ uncertainty shown in parentheses). Our experimental value of 2053.172043(11) cm^{-1} for the intercept at zero pressure is in good agreement with the line center frequency of 2053.172006(1) cm^{-1} obtained from heterodyne measurements [12,13] considering that our statistical error for the intercept does not include calibration and other experimental uncertainties that could contribute to the discrepancy. The measured N_2- and O_2- and calculated air-shift parameters (taken as $\delta^{Air}=0.79\delta^{N_2}+0.21\delta^{O_2}$) are also listed in Table 1. In this case, no corrections were made for variations in room temperature over the range from 22.0 to 25.5 °C because no data on the temperature dependence of OCS pressure shifts are currently available. However, an estimate based on the temperature exponent of 0.4×10^{-5} cm^{-1} atm^{-1} K^{-1} for HCN in [25] gives a negligible correction of the order of only 10^{-5} cm^{-1} atm^{-1}.

In contrast to the pressure broadening results, our values for the pressure lineshift coefficients do not show any systematic dependence on $|m|$, as seen in Fig. 11. This may be because the lineshifts are small and are highly sensitive to calibration, background and other experimental uncertainties as well as the effects of line overlap and the model

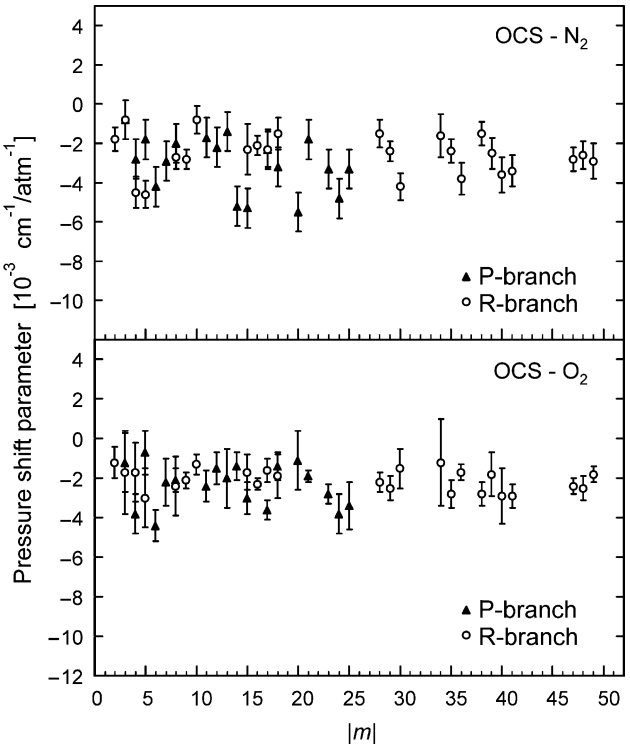

Fig. 11. N_2 and O_2 pressure-induced shift coefficients for OCS as a function of $|m|$.

function used. The substantial scatter in the values in Fig. 11 reflects this sensitivity. Nevertheless, all of the observed transitions of the band displayed negative shifts in line centers, varying from about -0.0008 to $-0.0055\ cm^{-1}\ atm^{-1}$. The mean values of the N_2-, O_2- and air-shift parameters were obtained as $-0.0028(12)$, $-0.0022(8)$ and $-0.0026(10)\ cm^{-1}\ atm^{-1}$, respectively. In comparison, the N_2- and O_2-pressure line shifts reported in [17] for the $2\nu_3$ band of OCS have the same negative sign but slightly higher magnitudes ranging from $-0.0015\ cm^{-1}\ atm^{-1}$ at low $|m|$ to $-0.006\ cm^{-1}\ atm^{-1}$ for high $|m|$.

4. A note on line intensities

Since our work was not originally aimed at line intensity measurement, the OCS pressures in the sample cell were not precisely controlled for the different target transitions but were just set at appropriate values in order to give a good *S*/*N* ratio for an observed line while keeping the effects of saturation and self-broadening to a minimum. However, since the OCS partial pressure was fixed throughout the measurement cycle for a given target transition, a useful check for systematic errors could be obtained by examining whether the integrated intensity of that target OCS absorption line remained constant for different pressures of the foreign gas. Fig. 12 shows the measured integrated intensities of the $P(11)$, $P(21)$ and $R(40)$ OCS lines versus pressure. The values are constant to within a standard

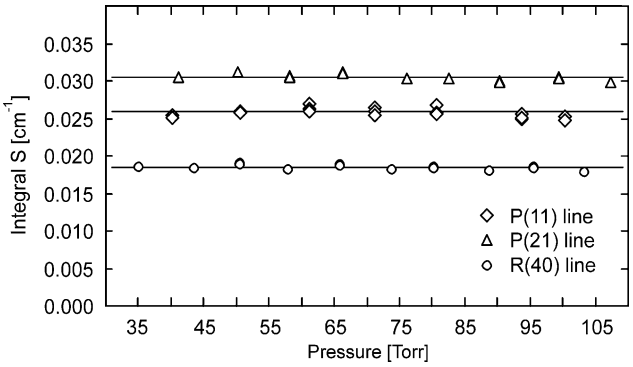

Fig. 12. Integrated intensities for the $P(11)$, $P(21)$ and $R(40)$ transitions of the ν_3 band of OCS at 296 K for fixed partial pressure of OCS and varying pressures of foreign gas. Solid horizontal lines represent mean experimental intensity values.

deviation of only 1–2%, indicating that our baselines were well determined and supporting the accuracy of our measurements and the validity of the data treatment. As a further test of our results, careful and well-calibrated intensity measurements were performed for the $P(11)$ OCS line. The integrated intensity was determined to be 0.766×10^{-18} cm/molecule, in agreement to better than 1% with the value of 0.759×10^{-18} cm/molecule given for this line in the HITRAN database.

5. Conclusions

The nitrogen and oxygen pressure broadening and shift coefficients of 42 transitions from the ν_3 band of $^{16}O^{12}C^{32}S$ have been measured at room temperature with a high-resolution IR TDL spectrometer over the quantum number range from $m=-25$ for the P-branch to $m=49$ for the R-branch. The corresponding coefficients for OCS in dry air were calculated from the measured N_2 and O_2 values. As observed for other OCS vibrational bands, the ν_3 pressure broadening parameters decrease markedly as $|m|$ increases. Good agreement was found, both for the absolute values and for the $|m|$-dependence, with coefficients reported previously for the ν_1 and $2\nu_3$ bands [15–17]. The ratio of O_2- to N_2-broadening coefficients at room temperature also varies significantly with $|m|$, decreasing from 0.882 at low $|m|$ down to 0.844 for $|m|=50$. The difference between N_2- and O_2-broadening parameters is equal to $0.0127(3)\ cm^{-1}\ atm^{-1}$ and is independent of $|m|$ to within experimental error.

In an examination of pressure-induced shifts, small negative shifts of the line center positions varying linearly with pressure were observed and are in reasonable agreement with those reported previously for the $2\nu_3$ band [18].

Our measured air–pressure broadening parameters show some significant differences from the values reported in the GEISA and HITRAN databases, particularly at high rotational quantum number $|m|$. Thus, our results should serve as useful updates for database improvement, as our

measurements of the N_2- and O_2-pressure broadening parameters of OCS transitions appear to be the most systematic and accurate available at the present time for the ν_3 band.

Examination of integrated intensities for several test transitions showed that the values were independent of the pressure of the foreign perturbing gas to within about 1–2%. A carefully controlled measurement for the $P(11)$ transition gave an integrated intensity of 0.766×10^{-18} cm/molecule in good agreement with the value of 0.759×10^{-18} cm/molecule reported for this line in the HITRAN database. The demonstration of the possibility of measuring the integrated intensities of spectral lines with accuracy better than 1% is very important for analytical applications of our spectrometer.

In conclusion, we believe that our results represent useful additions to current standard reference data for line broadening in OCS. They should also be of significance for fundamental theoretical line broadening calculations and for application in spectroscopic and remote sensing observations of OCS in the terrestrial environment and in astronomical sources.

Acknowledgements

We are pleased to dedicate this work to Jean Demaison, in recognition of his long and distinguished career in high-resolution molecular spectroscopy and his many important contributions to the field. L.-H.X. and R.M.L. are grateful for financial support for this research from the Canadian Institute for Photonic Innovations (CIPI), under the national Networks of Centres of Excellence Programme, and the Natural Sciences and Engineering Research Council of Canada. M.K. and M.Y.T. acknowledge partial support from the Russian Foundation for Basic Research and the Russian Ministry of Industry, Science and Technologies. We thank D. Hurtmans for his contributions to the design and development of the data multiplexing and acquisition capabilities of the spectrometer and to the data-handling program, and I. Leonov, E.H. Leung and P. Wang for their further contributions to the data capture and processing software.

References

[1] S.F. Watts, Atmos. Environ. 34 (2000) 761.
[2] A. Goldman, M.T. Coffey, T.M. Stephen, C.P. Rinsland, W.G. Mankin, J.W. Hannigan, J. Quant. Spectrosc. Radiat. Transfer 67 (2000) 447.
[3] N.J. Blake, D.G. Streets, J.H. Woo, I.J. Simpson, J. Green, S. Meinardi, K. Kita, E. Atlas, H.E. Fuelberg, G. Sachse, M.A. Avery, S.A. Vay, R.W. Talbot, J.E. Dibb, A.R. Bandy, D.C. Thornton, F.S. Rowland, D.R. Blake, J. Geophys. Res. 109 (2004) (Art. No. D15S05).
[4] C.P. Rinsland, A. Goldman, E. Mahieu, R. Zander, J. Notholt, N.B. Jones, D.W.T. Griffith, T.M. Stephen, L.S. Chiou, J. Geophys. Res. 107 (2002) (Art. No. 4657).
[5] C.P. Rinsland, R. Zander, E. Mahieu, P. Demoulin, A. Goldman, D.H. Ehhalt, J. Rudolph, J. Geophys. Res. 97 (2002) 5995.
[6] J.B. Pollack, J.B. Dalton, D. Grinspoon, R.B. Wattson, R. Freedman, D. Crisp, D.A. Allen, B. Bezard, C. DeBergh, L.P. Giver, Q. Ma, R. Tipping, Icarus 103 (1993) 1.
[7] B. Bezard, C. DeBergh, D. Crisp, J.P. Maillard, Nature 345 (1990) 508.
[8] N.J. Evans, J.H. Lacy, J.S. Carr, Astrophys. J. 383 (1991) 674.
[9] L.M. Woodney, J. McMullin, M.F. Ahearn, Planet. Space Sci. 45 (1997) 717.
[10] N. Dello Russo, M.A. DiSanti, M.J. Mumma, K. Magee-Sauer, T.W. Rettig, Icarus 135 (1998) 377.
[11] T. Encrenaz, E. Lellouch, S.K. Atreya, A.S. Wong, Planet. Space Sci. 52 (2004) 1023.
[12] M. Murtz, P. Palm, W. Urban, A.G. Maki, J. Mol. Spectrosc. 204 (2000) 281.
[13] A.G. Maki, J.S. Wells, Wavenumber calibration tables from heterodyne frequency measurements NIST Special Publication 821, US Department of Commerce, Washington, DC, 1991 (http://physics.nist.gov/PhysRefData/wavenum/html/spect.html).
[14] L. Régalia-Jarlot, A. Hamdouni, X. Thomas, P. Von der Heyden, A. Barbe, J. Quant. Spectrosc. Radiat. Transfer 74 (2002) 455.
[15] A. Mouchet, G. Blanquet, P. Herbin, J. Walrand, C.P. Courtoy, J.P. Bouanich, Canad. J. Phys. 63 (1985) 527.
[16] J.P. Bouanich, J. Walrand, S. Alberty, G. Blanquet, J. Mol. Spectrosc. 123 (1987) 37.
[17] J.L. Domenech, D. Bermejo, J.P. Bouanich, J. Mol. Spectrosc. 200 (2000) 266.
[18] N. Jacquinet-Husson, N.A. Scott, A. Chédin, A.A. Chursin, Atmos. Oceanic Opt. 16-3 (2003) 256 (available from http://ara.lmd.polytechnique.fr/geisa).
[19] L.S. Rothman, D. Jacquemart, A. Barbe, D.C. Benner, M. Birk, L.R. Brown, M.R. Carleer, C. Chakerian, Jr., K. Chance, V. Dana, V.M. Devi, J.-M. Flaud, R.R. Gamache, A. Goldman, J.-M. Hartmann, K.W. Jucks, A.G. Maki, J.-Y. Mandin, S.T. Massie, J. Orphal, A. Perrin, C.P. Rinsland, M.A.H. Smith, J. Tennyson, R.N. Tolchenov, R.A. Toth, J. Vander Auwera, P. Varanasi, G. Wagner, The HITRAN 2004 molecular spectroscopic database, J. Quant. Spectrosc. Radiat. Transfer 96 (2005) 139.
[20] A. Perrin, Spectroscopy from Space in: J. Demaison, K. Sarka, E.A. Cohen (Eds.), NATO Science Series II vol. 20, Kluwer, Dordrecht, 2001, pp. 235–258.
[21] L.-H. Xu, R.M. Lees, G. Moruzzi, J. Mol. Spectrosc. 66 (1994) 338.
[22] M.R. De Backer-Barilly, B. Parvitte, X. Thomas, V. Zeninari, D. Courtois, J. Quant. Spectrosc. Radiat. Transfer 59 (1998) 345.
[23] C. Puzzarini, L. Dore, G. Cazzoli, J. Mol. Spectrosc. 216 (2002) 428.
[24] L. Galatry, Phys. Rev. 122 (1961) 1218.
[25] C.P. Rinsland, V. Malathy Devi, M.A.H. Smith, D.C. Benner, S.W. Sharpe, R.L. Sams, J. Quant. Spectrosc. Radiat. Transfer 82 (2003) 343.